RESEARCH ARTICLE • OPEN ACCESS

Mathematical Analysis of Typhoid Fever Dynamics with Age-Structured Control Measures

Mutairu Kayode Kolawole, Rasheed Gbemisola Ayoola, and Folasade Ajimot Adebisi

JAMBURA JOURNAL OF MATHEMATICS

Volume 8, Issue 1, Pages 126–137, February 2026

Received 10 November 2025, Revised 26 January 2026, Accepted 4 February 2026, Published 28 February 2026

To Cite this Article : M. K. Kolawole, R. G. Ayoola, and F. A. Adebisi,"Mathematical Analysis of Typhoid Fever Dynamics with Age-Structured Control Measures", *Jambura J. Math*, vol. 8, no. 1, pp. 126–137, 2026, *https://doi.org/10.37905/jjom.v8i1.35225*

JOURNAL INFO • JAMBURA JOURNAL OF MATHEMATICS

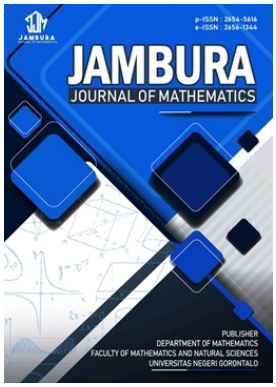

Homepage	:	http://ejurnal.ung.ac.id/index.php/jjom/index
Journal Abbreviation	:	Jambura J. Math.
Frequency	:	Biannual (February and August)
Publication Language	:	English (preferable), Indonesia
DOI	:	https://doi.org/10.37905/jjom
Online ISSN	:	2656-1344
Editor-in-Chief	:	Hasan S. Panigoro
Publisher	:	Department of Mathematics, Universitas Negeri Gorontalo
Country	:	Indonesia
OAI Address	:	http://ejurnal.ung.ac.id/index.php/jjom/oai
Google Scholar ID	:	iWLjgaUAAAAJ
Email	:	info.jjom@ung.ac.id

JAMBURA JOURNAL • FIND OUR OTHER JOURNALS

Jambura Journal of Biomathematics

Jambura Journal of Mathematics Education

Jambura Journal of Probability and Statistics

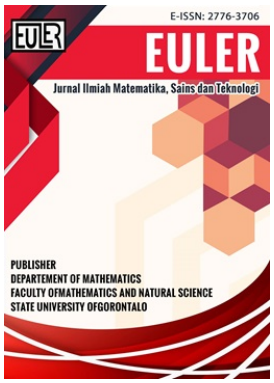

EULER : Jurnal Ilmiah Matematika, Sains, dan Teknologi

Jambura Journal of Mathematics, Volume 8, Issue 1, Pages 126–137, February 2026 https://doi.org/10.37905/jjom.v8i1.35225

Research Article

Check for updates

Mathematical Analysis of Typhoid Fever Dynamics with Age-Structured Control Measures

Mutairu Kayode Kolawole[1], **Rasheed Gbemisola Ayoola**[1,*], **Folasade Ajimot Adebisi**[1]

[1]*Department of Mathematical Sciences, Faculty of Basic and Applied Sciences, Osun State University, Osogbo, Nigeria*

ARTICLE HISTORY
Received 10 November 2025
Revised 26 January 2026
Accepted 4 February 2026
Published 28 February 2026

KEYWORDS
Typhoid outbreaks
Age-structure
Basic reproduction number
Homotopy perturbation method
Sensitivity analysis

ABSTRACT. *This research develops a mathematical model to investigate the dynamics of typhoid fever by incorporating age structure, vaccination and treatment strategies. Recognizing that different age groups display varying susceptibility and contact rates, the model provides a detailed representation of transmission. The analysis is to emphasize how vaccination programs and treatment interventions, when tailored to age-specific characteristics, can significantly reduce transmission and control outbreaks. The system of nonlinear differential equations describing the disease dynamics is analyzed and solved using the homotopy perturbation method. This analytical approach allows for an approximation of solutions while capturing the nonlinear interactions within the system. Sensitivity analysis is carried out to determine the most influential parameters on disease spread, particularly those affecting the basic reproduction number. The simulations reveal that increasing vaccination coverage and treatment rates leads to a decline in typhoid fever cases across all age groups. Age-targeted interventions are shown to enhance the effectiveness of control strategies compared with uniform measures. Sensitivity analysis result further indicate that parameters such as vaccination rate, treatment efficacy and contact patterns play vital roles in disease progression and a potential for its eradication.*

1. Introduction

Mathematical modeling is a crucial tool for understanding the transmission dynamics of infectious diseases like typhoid fever, a bacterial infection caused by *Salmonella typhi*. Typhoid fever is a public health concern in areas with poor sanitation and contaminated water, with symptoms such as high fever, abdominal pain, and gastrointestinal distress. If left untreated, it can lead to severe complications or death [1]. Recent advancements in modeling have incorporated factors such as age structure, vaccination, and treatment effects. Several researchers have conducted studies on mathematical modeling of typhoid fever dynamics using various analytical and numerical approaches [2–9].

The homotopy perturbation method has been particularly effective in solving differential equations that describe disease dynamics [10]. Including age structure allows models to more accurately capture the transmission patterns and the effectiveness of interventions like vaccination in different demographic groups [11]. Vaccination and treatment are key components in controlling typhoid fever. Vaccination reduces the susceptible population, while treatment helps alleviate symptoms and prevent complications. Modeling these interventions helps researchers evaluate the effectiveness of control measures and optimize strategies [12].

Children are especially vulnerable to severe illness and mortality from typhoid fever, and they can serve as reservoirs for transmission. Population dynamics, including factors like migration and urbanization, also affect the spread of the disease. Models that incorporate these factors provide insights into the long-term trends of disease transmission [13, 14]. Recent research studies have extensively used fractional-order and nonlinear epidemic models to examine disease dynamics, stability properties, and control strategies for infectious diseases such as monkeypox, Lassa fever, and leptospirosis [15–19].

Overall, mathematical models combining epidemiological data, age-specific factors, and interventions provide valuable insights into typhoid fever dynamics. These models aid in evidence-based decision-making, contributing to the effective control of typhoid fever and other infectious diseases [20]. Efforts to control typhoid outbreaks typically involve a combination of preventive and responsive measures aimed at interrupting the transmission of the bacterium and treating infected individuals. Water and sanitation interventions play a crucial role in preventing typhoid transmission and reducing the burden of the disease. Recent control measures for typhoid include [21, 22].

Improved Water and Sanitation Infrastructure: Investing in infrastructure for clean water supply, sanitation facilities, and proper waste management is fundamental in preventing typhoid outbreaks. Providing access to safe drinking water and promoting hygienic practices, such as hand washing and proper food handling, can significantly reduce the risk of typhoid transmission. Vaccination Campaigns: oral typhoid vaccines (TCVs) have been developed and deployed in typhoid-endemic areas as part of targeted vaccination campaigns. TCVs can provide short- to medium-term protection against typhoid and are often used in

*Corresponding Author.

Email : *ayoolarasheed96@gmail.com* (R. G. Ayoola)
Homepage : http://ejurnal.ung.ac.id/index.php/jjom/index / E-ISSN : 2656-1344

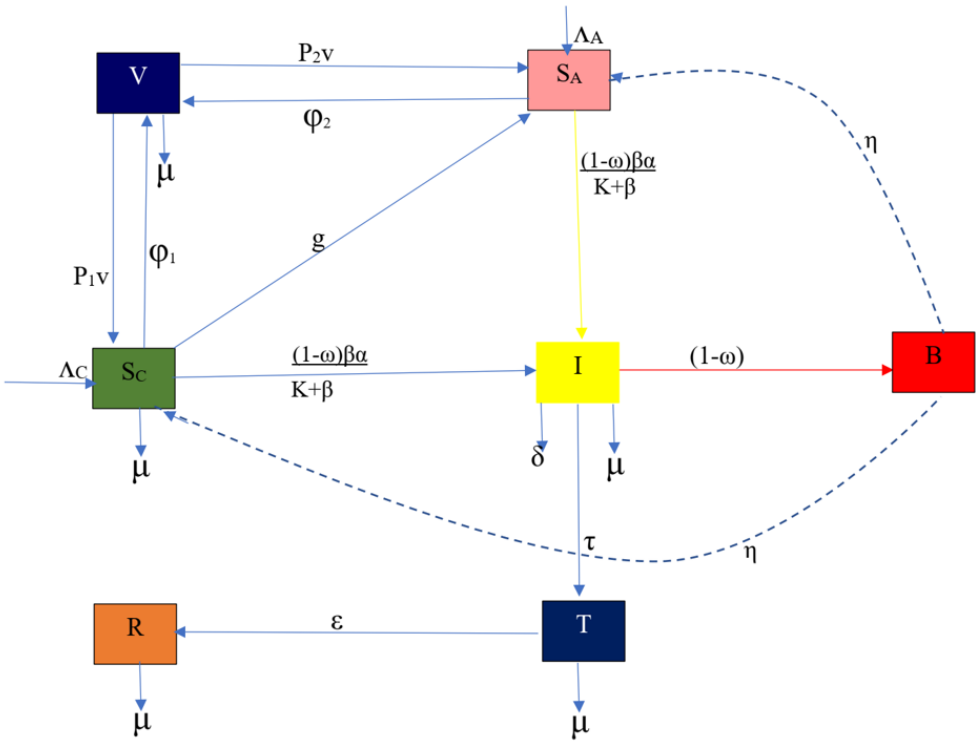

Figure 1. Model diagram showing the transmission dynamics of typhoid fever with age structure and vaccination

outbreak response efforts and in areas with a high risk of typhoid transmission [23].

Surveillance and early detection: Strengthening surveillance systems for typhoid and enhancing early detection and response mechanisms are critical for containing outbreaks and preventing the spread of the disease. Rapid diagnostic tests, along with effective reporting and monitoring systems, enable health authorities to identify and respond to typhoid cases promptly [24]. Health education and community engagement in promoting awareness about typhoid transmission, symptoms, and preventive measures through health education campaigns can empower communities to take proactive steps in preventing the disease. Engaging with community leaders and stakeholders fosters community participation and ownership of typhoid control efforts, leading to sustainable outcomes.

Treatment and case management: Providing prompt and appropriate treatment for typhoid cases is essential for reducing morbidity and mortality associated with the disease, along with the administration of antibiotics in severe cases. Ensuring access to healthcare facilities equipped to manage typhoid cases helps prevent complications and reduce the spread of the disease [25].

Integrated Approach: Implementing a multi-sectorial and integrated approach to typhoid control, involving collaboration between health authorities, water and sanitation agencies, non-governmental organizations, and other stakeholders, is essential for addressing the complex determinants of typhoid transmission. Coordinated efforts across various sectors can maximize the impact of control measures and contribute to sustainable typhoid prevention and control strategies [26].

2. Model

2.1. Model Formulation

We develop a model with a bacteria population N_B, denoted by $B(t)$, and a human population N_H. The populations are subdivided into different epidemiological classes: susceptible children (S_C), susceptible adults (S_A), vaccinated individuals (V), infected individuals (I), treated individuals (T), recovered individuals (R), and bacteria population in the environment (B).

The model assumes that the human population is recruited into the susceptible compartment of children at the rate Λ_C, and into the susceptible compartment of adults at the rate Λ_A. Susceptible individuals are infected at the rate $\frac{\alpha B}{K+B}$, where α is the rate of *Salmonella Typhi* contamination in foods and drinks, and $\frac{B}{K+B}$ is the probability of individuals consuming foods or drinks contaminated with typhoid-causing bacteria.

All human populations experience natural death at the rate μ, and infected individuals die from typhoid at the rate δ. The treatment rate of infected individuals is represented by τ. Excretion of *Salmonella Typhi* bacteria by infected children and adults into the environment occurs at the rate η, and the bacteria die in the environment at the rate υ. The parameter ω represents the hygiene rate, ψ_1 and ψ_2 denote the vaccination rates of children and adults respectively, while ρ_1 and ρ_2 represent the waning rates of immunity. The parameter g represents the rate at which children become adults.

The assumed parameter values were chosen to correspond to biologically reasonable ranges found in age-structured and environmentally mediated typhoid transmission studies. When direct empirical estimates were not available, conservative values typically employed in the epidemiological modeling litera-

Table 1. Description of state variables

Variable	Description
$S_C(t)$	Number of susceptible children
$S_A(t)$	Number of susceptible adults
$V(t)$	Number of vaccinated individuals
$I(t)$	Number of infected individuals
$T(t)$	Number of treated individuals
$R(t)$	Number of recovered individuals
$B(t)$	Concentration of *Salmonella Typhi* bacteria in the environment

Table 2. Parameter values and references

Parameter	Description	Value	References
ω	Hygiene rate	0.3	[14]
δ	Disease-induced death rate	0.015	[26]
ρ_1, ρ_2	Waning rate of immunity (children, adults)	0.0186821	[25]
μ	Natural death rate	$1/60{,}000$	[1]
η	Excretion rate of *Salmonella Typhi* by infected humans	0.003	[13]
τ	Treatment rate of infected individuals	0.00174478	[23]
ε	Recovery rate of treated individuals	0.00331428	[10]
ψ_1, ψ_2	Vaccination rate of children and adults	0.0002	[27]
g	Rate at which children become adults	0.01	Assumed
K	Half-saturation constant in $\lambda(B) = \dfrac{\alpha B}{K+B}$	50,000	Assumed
α	Transmission scaling factor in $\lambda(B)$	10	[11]
Λ_C, Λ_A	Recruitment rates of children and adults	150,000; 1854	[21]
v	Natural death rate of *Salmonella Typhi* in the environment	0.001	Assumed

ture were selected to provide realistic disease dynamics and numerical stability.

The diagram in Figure 1 represents the model flowchart and the model equation is presented in eq. (1). The model variables are described in the Table 1, while the models parameter values are presented in the Table 2.

$$\begin{cases} \dfrac{dS_C}{dt} = \Lambda_C - (1-\omega)\,\lambda(B)\,S_C - (\mu+\psi_1)S_C - gS_C + \rho_1 V, \\ \dfrac{dS_A}{dt} = \Lambda_A - (1-\omega)\,\lambda(B)\,S_A - (\mu+\psi_2)S_A + gS_C + \rho_2 V, \\ \dfrac{dV}{dt} = \psi_1 S_C + \psi_2 S_A - (\rho_1+\rho_2)V - \mu V, \\ \dfrac{dI}{dt} = (1-\omega)\,\lambda(B)\,(S_C+S_A) - (\mu+\delta+\tau)I, \\ \dfrac{dT}{dt} = \tau I - (\varepsilon+\mu)T, \\ \dfrac{dR}{dt} = \varepsilon T - \mu R, \\ \dfrac{dB}{dt} = (1-\omega)\,\eta I - vB, \end{cases} \tag{1}$$

where $\lambda_A = \lambda_C = \dfrac{\alpha B}{K+B}$ is the common *force of infection* for both children and adults. The force of infection in eq. (1) is expressed as

$$\lambda(B) = \frac{\alpha B}{K+B}.$$

2.2. Model's Limitations

The suggested model has some simplifying assumptions, which may limit its scope. The population is classified into only two age groups, which may not adequately capture variation in contact patterns, immunity, and behavior among finer age categories. Homogeneous mixing is assumed inside compartments, while real populations frequently exhibit spatial and social heterogeneity. Environmental transmission is represented by a single bacterial compartment with constant shedding and decay rates, ignoring seasonal variation and changes in water and sanitation conditions. Vaccination and therapy are considered to be equally effective across age groups, with declining immunity estimated using constant rates. Finally, the Homotopy Perturbation Method is a local approximation that requires numerical confirmation for long-term dynamics.

3. Results and Discussion

3.1. Existence and Uniqueness of Model Solution

Feasible Region: We first determine the feasible region in which the model solution is biologically meaningful and bounded. The total human population N_H is given by eq. (2)

$$N_H = S_C + S_A + V + I + T + R. \tag{2}$$

Differentiating eq. (2) with respect to time and substituting the corresponding equations from the model gives

$$\frac{dN_H}{dt} = \Lambda - \mu N_H,$$

where $\Lambda = \Lambda_C + \Lambda_A$ represents the total recruitment rate into the human population.

By the method of integrating factors, the solution is obtained as given in eq. (3)

$$N_H(t) = N_H(0)e^{-\mu t} + \frac{\Lambda}{\mu}\left(1 - e^{-\mu t}\right). \tag{3}$$

At $t = 0$, from eq. (3), we have

$$N_H(0) = S_C(0) + S_A(0) + V(0) + I(0) + T(0) + R(0).$$

As $t \to \infty$, eq. (3) implies that $N_H(t) \to \frac{\Lambda}{\mu}$, implying that $N_H(t)$ is bounded.

The bacteria population $B(t)$ satisfies a similar equation of the form

$$\frac{dB}{dt} = (1-\omega)\eta I - vB,$$

whose solution by integrating factor is given as in eq. (4)

$$B(t) = B(0)e^{-vt} + \frac{(1-\omega)\eta I}{v}\left(1 - e^{-vt}\right). \tag{4}$$

Thus, the feasible region of the model is defined as in eq. (5).

$$\Omega = \{(S_C, S_A, V, I, T, R, B) \in \mathbb{R}^7_+ : N_H \le \tfrac{\Lambda}{\mu},\ B \le \tfrac{(1-\omega)\eta N_H}{v}\}. \tag{5}$$

Hence, Ω is positively invariant and attracts all trajectories starting in $\mathbb{R}^7_+$. Therefore, the model is *epidemiologically and mathematically well-posed*. It suffices to study the system dynamics in Ω.

3.2. Positivity and Boundedness of Model Solutions

We assume that all initial conditions are nonnegative. The following theorem establishes that the solutions of the model remain positive for all $t \ge 0$.

Theorem 1. *Let Ω be defined by eq. (5). Then, the solution of the model is positive for all $t \ge 0$, that is, as stated in eq. (6).*

$$S_C(t),\ S_A(t),\ V(t),\ I(t),\ T(t),\ R(t),\ B(t) > 0. \tag{6}$$

Proof. From the system of differential equations, consider the first equation for $S_C(t)$. Using the integrating factor $e^{\mu t}$, we obtain

$$S_C(t) = S_C(0)e^{-\mu t} + \int_0^t e^{-\mu(t-s)}(\Lambda_C - \beta S_C B)\, ds. \tag{7}$$

Since all terms on the right-hand side are nonnegative, it follows that $S_C(t) > 0$. Similarly, for the adult susceptible class, integrating gives

$$S_A(t) = S_A(0)e^{-\mu t} + \int_0^t e^{-\mu(t-s)}(gS_C - \beta S_A B)\, ds > 0. \tag{8}$$

For the vaccinated class, it follows that eq. (9) holds

$$V(t) = V(0)e^{-(\rho_1+\rho_2+\mu)t} + \int_0^t e^{-(\rho_1+\rho_2+\mu)(t-s)}(\psi_1 S_C + \psi_2 S_A)\, ds > 0. \tag{9}$$

For the infected class, eq. (10) gives

$$I(t) = I(0)e^{-(\tau+\delta+\mu)t} + \int_0^t e^{-(\tau+\delta+\mu)(t-s)}\beta(S_C+S_A)B\, ds > 0. \tag{10}$$

Therefore, all state variables remain positive for $t \ge 0$, proving the theorem. □

3.3. Basic Reproduction Number (R_*)

There are two disease-related compartments (I and B), but new infections arise only through contact with the environmental bacteria compartment. Hence, only the infected class I and the bacteria class B are involved in the computation of the basic reproduction number R_*.

We define R_* using the next-generation matrix approach [28–30]:

$$R_* = \rho(FV^{-1}),$$

where $\rho(\cdot)$ denotes the spectral radius of the matrix product FV^{-1}.

Let F represent the rate of appearance of new infections in each infected compartment, and V represent the rate of transfer of individuals into and out of these compartments due to other processes.

At the disease-free equilibrium E_0, we have:

$$F_i = \left[\frac{\partial \mathcal{F}_i(x_0)}{\partial x_j}\right], \qquad V_i = \left[\frac{\partial \mathcal{V}_i(x_0)}{\partial x_j}\right],$$

where $\mathcal{F}_i$ denotes new infection terms, and $\mathcal{V}_i$ denotes transitions between compartments.

Infection subsystem:

From the model, we consider the infected and bacterial dynamics:

$$\frac{dI}{dt} = (1-\omega)\lambda(B)(S_C + S_A) - (\mu+\delta+\tau)I,$$
$$\frac{dB}{dt} = (1-\omega)\eta I - vB.$$

At the DFE, $\lambda(B) = \frac{\alpha B}{K+B} \approx \frac{\alpha B}{K}$ (since $B \to 0$). Hence, the linearized infection subsystem becomes:

$$\frac{d}{dt}\begin{pmatrix} I \\ B \end{pmatrix} = \underbrace{\begin{pmatrix} 0 & (1-\omega)\dfrac{\alpha(S_{C_0}+S_{A_0})}{K} \\ (1-\omega)\eta & 0 \end{pmatrix}}_{F} \begin{pmatrix} I \\ B \end{pmatrix} - \underbrace{\begin{pmatrix} \mu+\delta+\tau & 0 \\ 0 & v \end{pmatrix}}_{V} \begin{pmatrix} I \\ B \end{pmatrix}.$$

Next-generation matrix:

Thus,

$$FV^{-1} = \begin{pmatrix} 0 & \dfrac{(1-\omega)\alpha(S_{C_0}+S_{A_0})}{Kv} \\ \dfrac{(1-\omega)\eta}{\mu+\delta+\tau} & 0 \end{pmatrix}.$$

The eigenvalues of FV^{-1} are given by $\pm\sqrt{ab}$, where

$$a = \frac{(1-\omega)\alpha(S_{C_0}+S_{A_0})}{Kv},$$

$$b = \frac{(1-\omega)\eta}{\mu+\delta+\tau}.$$

Hence, the basic reproduction number is presented in eq. (11).

$$R_* = \sqrt{ab} = (1-\omega)\sqrt{\frac{\alpha\eta(S_{C_0}+S_{A_0})}{K\,v\,(\mu+\delta+\tau)}}. \tag{11}$$

This expression quantifies the expected number of secondary infections generated by a single infected individual in a completely susceptible population.

3.4. Local Stability of the Disease-Free Equilibrium

Theorem 2. *The disease-free equilibrium (DFE) is locally asymptotically stable if $R_* < 1$ and unstable if $R_* > 1$.*

Proof. Let $J(E_0)$ be the Jacobian matrix of the full system evaluated at the disease-free equilibrium E_0. This matrix is obtained by linearizing system (1) about E_0.

$$J(E_0) = \begin{pmatrix} J_{11} & 0 & \rho_1 & 0 & 0 & 0 & 0 \\ g & J_{22} & \rho_2 & 0 & 0 & 0 & 0 \\ \psi_1 & \psi_2 & J_{33} & 0 & 0 & 0 & 0 \\ 0 & 0 & 0 & J_{44} & 0 & 0 & 0 \\ 0 & 0 & 0 & \tau & J_{55} & 0 & 0 \\ 0 & 0 & 0 & 0 & \varepsilon & -\mu & 0 \\ 0 & 0 & 0 & J_{74} & 0 & 0 & -v \end{pmatrix}, \tag{12}$$

where

$$\begin{aligned} J_{11} &= -(\mu+\psi_1+g), \\ J_{22} &= -(\mu+\psi_2) \\ J_{33} &= -(\rho_1+\rho_2+\mu), \\ J_{44} &= -(\mu+\delta+\tau) \\ J_{55} &= -(\varepsilon+\mu) \\ J_{74} &= (1-\omega)\eta. \end{aligned}$$

The characteristic equation is obtained from

$$|J(E_0) - \lambda I| = 0.$$

Because the Jacobian is block lower-triangular, the eigenvalues are simply the diagonal entries given in eq. (13).

$$\begin{aligned} \lambda_1 &= -(\mu+\psi_1+g), \\ \lambda_2 &= -(\mu+\psi_2), \\ \lambda_3 &= -(\rho_1+\rho_2+\mu), \\ \lambda_4 &= -(\mu+\delta+\tau), \\ \lambda_5 &= -(\varepsilon+\mu), \\ \lambda_6 &= -\mu, \\ \lambda_7 &= -v. \end{aligned} \tag{13}$$

All eigenvalues are negative provided $R_* < 1$, implying that the DFE is locally asymptotically stable. So, the disease-free equilibrium is locally asymptotically stable if $R_* < 1$, and unstable if $R_* > 1$. □

This condition represents the epidemiological threshold for the persistence of typhoid infection in the population.

3.5. Local Stability of the Endemic Equilibrium

Theorem 3. *The endemic equilibrium of the proposed epidemic model is locally asymptotically stable if $R_* > 1$ and unstable otherwise ($R_* < 1$).*

Proof. To examine the local stability near the endemic equilibrium $E^* = (S_C^*, S_A^*, V^*, I^*, T^*, R^*, B^*)$, we linearize the system about E^*. Let

$$\begin{aligned} S_C &= a + S_C^*, \quad & S_A &= b + S_A^*, \\ V &= c + V^*, \quad & I &= e + I^*, \\ T &= x + T^*, \quad & R &= y + R^*, \\ B &= z + B^*, \end{aligned}$$

where a, b, c, e, x, y, z represent small perturbations around the endemic equilibrium values.

Substituting these into the system of equations and neglecting higher-order nonlinear terms gives the linearized system:

$$\begin{aligned} \frac{da}{dt} &= \Lambda_C - (1-\omega)\lambda_C z a - (1-\omega)\lambda_C z b - (\mu+\psi_1)a \\ &\quad + \rho_1 c - g a, \\ \frac{db}{dt} &= \Lambda_A - (1-\omega)\lambda_A z a - (1-\omega)\lambda_A z b - (\mu+\psi_2)b \\ &\quad + \rho_2 c + g a, \\ \frac{dc}{dt} &= \psi_1 a + \psi_2 b - (\rho_1+\rho_2+\mu)c, \\ \frac{de}{dt} &= (1-\omega)\lambda_C z a + (1-\omega)\lambda_A z b - (\mu+\delta+\tau)e, \\ \frac{dx}{dt} &= \tau e - (\varepsilon+\mu)x, \\ \frac{dy}{dt} &= \varepsilon x - \mu y, \\ \frac{dz}{dt} &= (1-\omega)\eta e - v z. \end{aligned}$$

The divergence of the Dulac function $G(X)$ multiplied by the system's vector field is given by

$$\frac{d}{dt}(GX) = \sum_{i=1}^{7} \frac{\partial}{\partial x_i}\left(G\frac{dx_i}{dt}\right),$$

where $x_i \in \{S_C, S_A, V, I, T, R, B\}$.

Substituting the above components and differentiating with respect to each state variable, we obtain

$$\begin{aligned} \frac{d}{dt}(GX) &= \frac{\partial}{\partial S_C}\left(-\frac{\Lambda_C}{S_C S_A} - \frac{(\mu+\psi_1)}{S_A} - \frac{g}{S_A}\right) \\ &\quad + \frac{\partial}{\partial S_A}\left(-\frac{(\mu+\psi_2)}{S_C S_A}\right) + \frac{\partial}{\partial V}\left(-\frac{(\rho_1+\rho_2+\mu)V}{S_C S_A}\right) \\ &\quad + \frac{\partial}{\partial I}\left(-\frac{(\mu+\delta+\tau)}{S_C S_A}\right) + \frac{\partial}{\partial T}\left(-\frac{(\varepsilon+\mu)T}{S_C S_A}\right) \\ &\quad + \frac{\partial}{\partial R}\left(-\frac{\mu R}{S_C S_A}\right) + \frac{\partial}{\partial B}\left(-\frac{vB}{S_C S_A}\right). \end{aligned}$$

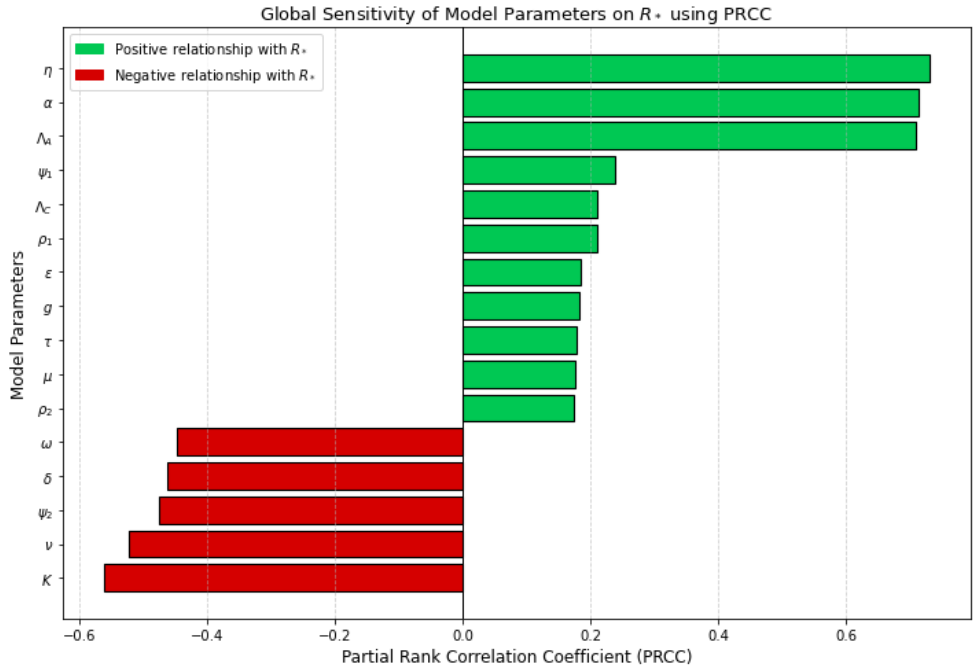

Figure 2. Global sensitivity analysis using Partial Rank Correlation Coefficients (PRCC). Parameters with positive PRCC values enhance R_* when increased (green bars), while those with negative PRCC values reduce R_* (red bars)

Evaluating these derivatives, we have

$$\frac{d}{dt}(GX) = -\frac{1}{S_C S_A}\Big[\Lambda_C + \Lambda_A + (\mu+\psi_1+g) + (\mu+\psi_2) + (\rho_1+\rho_2+\mu)V + (\mu+\delta+\tau) + (\varepsilon+\mu) + v\Big].$$

Clearly,

$$\frac{d}{dt}(GX) < 0 \quad \text{for all } S_C, S_A, V, I, T, R, B > 0.$$

Thus, the divergence of $G(X)$ multiplied by the system vector field is negative throughout the interior of the feasible region Ω. By the Dulac–Bendixson criterion, the system does not admit any periodic orbits in the interior of Ω, and all trajectories approach the unique endemic equilibrium E^*. Hence, the endemic equilibrium point E^* is *locally asymptotically stable* whenever $R_* > 1$. □

3.6. *Sensitivity Analysis*

Sensitivity analysis is performed to find which parameters significantly affect the basic reproduction number, R_*. The Partial Rank Correlation Coefficient (PRCC) method is used because it is robust in determining the strength and direction of the relationship between model parameters and the response variable while considering nonlinear relationships between parameters [31–33]. This analysis uses the Latin Hypercube Sampling (LHS) method to generate multiple parameter sets within a $\pm 30\%$ variation range of their baseline values. For each set of sampled parameters, the corresponding value of R_* is calculated using eq. (11), and PRCC values are then calculated in order to determine the monotonic correlation between each parameter and R_*. The PRCC values for each parameter, p_i, are denoted as ρ_i and range from $-1 \leq \rho_i \leq 1$. A positive PRCC value $(\rho_i > 0)$ signifies that an increase in the parameter increases R_*, and a negative PRCC $(\rho_i < 0)$ indicates that an increase in the parameter decreases R_*. The absolute value $|\rho_i|$ provides the influence strength, with values near 1 indicating strong and those near 0 indicating weak relationships.

The PRCC values illustrated in Figure 2 highlight a strong positive correlation of the transmission coefficient, α, bacterial shedding rate, η, and recruitment rate of children and adults, Λ_C and Λ_A, with R_*. Thus, high bacterial shedding, high transmission potential, and high recruitment into the susceptible classes significantly enhance the persistence of infection in the population. The hygiene rate, ω, vaccination rates in children and adults, ψ_1 and ψ_2, treatment rate, τ, and bacterial death rate, v, are strongly negatively correlated with R_*. This indicates that improved hygiene, higher vaccination coverage, successful treatment, and rapid bacterial decay in the environment effectively reduce disease transmission. In addition, the waning immunity parameters, ρ_1 and ρ_2, have weak positive correlations, reflecting that increased loss of immunity marginally enhances the disease reproduction potential. Therefore, this confirms that α, η, Λ_C, and Λ_A are the most influential determinants of typhoid transmission while ω, ψ_1, ψ_2, τ, and v are key intervention parameters in lowering the basic reproduction number and reducing the spread of typhoid fever.

3.7. *Homotopy Perturbation Method (HPM)*

In this section, the Homotopy Perturbation Method (HPM) is employed to obtain approximate analytical solutions of the typhoid fever model (system (1)). The method constructs correctional functionals for each differential equation in the system by introducing an embedding parameter $p \in [0, 1]$.

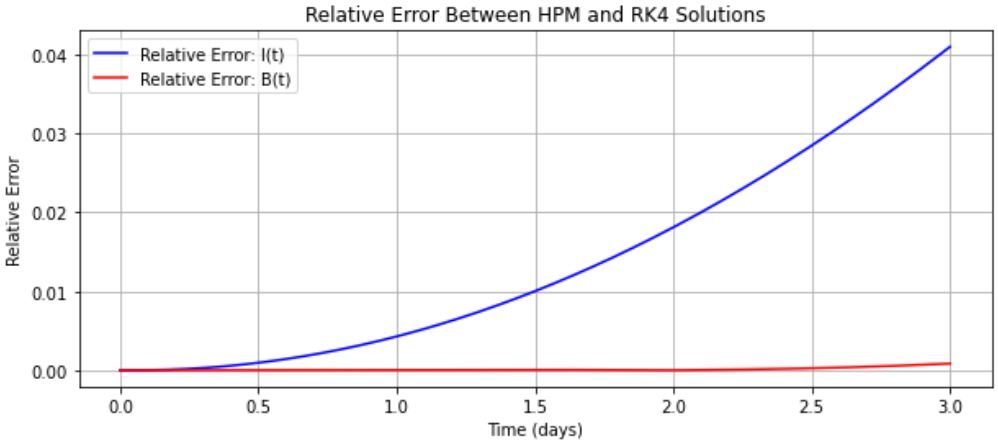

Figure 3. Relative error between the HPM approximate solutions and numerical Runge–Kutta solutions for infected individuals and bacterial concentration. The error remains small and bounded over the validation interval, confirming the accuracy of the HPM approximation

The corresponding homotopy equations are given as:

$$(1-p)\frac{dS_C}{dt} + p\left[\frac{dS_C}{dt} - \Big(\Lambda_C - (1-\omega)\lambda_C B(t)[S_C(t)+S_A(t)] - (\mu+\psi_1)S_C(t) - gS_C(t) + \rho_1 V(t)\Big)\right] = 0,$$

$$(1-p)\frac{dS_A}{dt} + p\left[\frac{dS_A}{dt} - \Big(\Lambda_A - (1-\omega)\lambda_A B(t)[S_C(t)+S_A(t)] - (\mu+\psi_2)S_A(t) + gS_C(t) + \rho_2 V(t)\Big)\right] = 0,$$

$$(1-p)\frac{dV}{dt} + p\left[\frac{dV}{dt} - \big(\psi_1 S_C(t) + \psi_2 S_A(t) - (\rho_1+\rho_2+\mu)V(t)\big)\right] = 0,$$

$$(1-p)\frac{dI}{dt} + p\left[\frac{dI}{dt} - \big((1-\omega)B(t)(S_C(t)+S_A(t))(\lambda_C+\lambda_A) - (\mu+\delta+\tau)I(t)\big)\right] = 0,$$

$$(1-p)\frac{dT}{dt} + p\left[\frac{dT}{dt} - (\tau I(t) - (\varepsilon+\mu)T(t))\right] = 0,$$

$$(1-p)\frac{dR}{dt} + p\left[\frac{dR}{dt} - (\varepsilon T(t) - \mu R(t))\right] = 0,$$

$$(1-p)\frac{dB}{dt} + p\left[\frac{dB}{dt} - \big((1-\omega)\eta I(t) - vB(t)\big)\right] = 0.$$

3.7.1. Expansion of the Solution Series

We assume that each state variable can be expressed as a power series in p:

$$S_C(t) = \sum_{n=0}^{\infty} p^n S_{Cn}(t), \quad S_A(t) = \sum_{n=0}^{\infty} p^n S_{An}(t),$$
$$V(t) = \sum_{n=0}^{\infty} p^n V_n(t), \quad I(t) = \sum_{n=0}^{\infty} p^n I_n(t),$$
$$T(t) = \sum_{n=0}^{\infty} p^n T_n(t), \quad R(t) = \sum_{n=0}^{\infty} p^n R_n(t),$$
$$B(t) = \sum_{n=0}^{\infty} p^n B_n(t).$$

Substituting these expansions into the homotopy equations and equating the coefficients of like powers of p, we obtain systems of equations for successive approximations.

3.7.2. Zeroth and First Approximations

At $n = 0$, the system reduces to

$$\frac{dS_{C0}}{dt} = 0, \quad \frac{dS_{A0}}{dt} = 0, \quad \frac{dV_0}{dt} = 0, \quad \frac{dI_0}{dt} = 0,$$
$$\frac{dT_0}{dt} = 0, \quad \frac{dR_0}{dt} = 0, \quad \frac{dB_0}{dt} = 0.$$

Thus, the zeroth-order solutions correspond to the initial conditions:

$$S_{C0}(t) = S_{C0}, \quad S_{A0}(t) = S_{A0}, \quad V_0(t) = V_0,$$
$$I_0(t) = I_0, \quad T_0(t) = T_0,$$
$$R_0(t) = R_0, \quad B_0(t) = B_0.$$

At $n = 1$, we have the first-order approximations:

$$S'_{C1}(t) = \Lambda_C - (1-\omega)\lambda_C B_0(S_{C0}+S_{A0}) - (\mu+\psi_1)S_{C0} - gS_{C0} + \rho_1 V_0,$$
$$S'_{A1}(t) = \Lambda_A - (1-\omega)\lambda_A B_0(S_{C0}+S_{A0}) - (\mu+\psi_2)S_{A0} + gS_{C0} + \rho_2 V_0,$$
$$V'_1(t) = \psi_1 S_{C0} + \psi_2 S_{A0} - (\rho_1+\rho_2+\mu)V_0,$$
$$I'_1(t) = (1-\omega)B_0(S_{C0}+S_{A0})(\lambda_C+\lambda_A) - (\mu+\delta+\tau)I_0,$$
$$T'_1(t) = \tau I_0 - (\varepsilon+\mu)T_0,$$
$$R'_1(t) = \varepsilon T_0 - \mu R_0,$$
$$B'_1(t) = (1-\omega)\eta I_0 - vB_0.$$

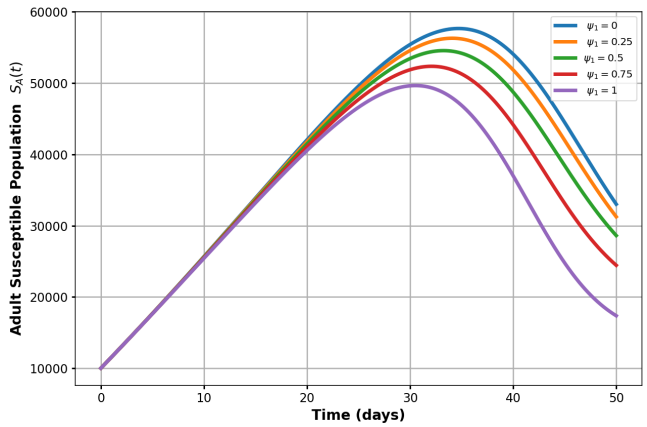

(a) Susceptible adults (S_A)

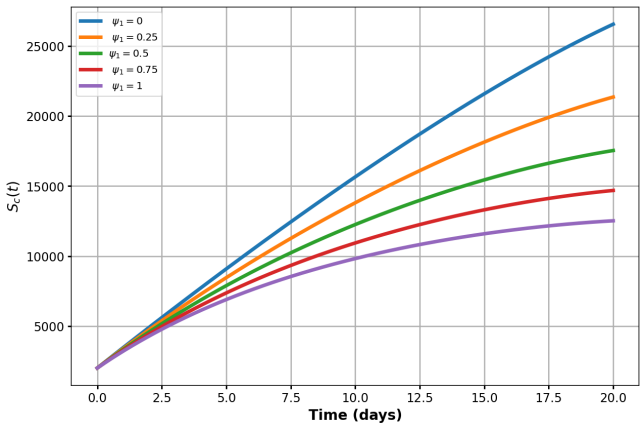

(b) Infected individuals (I)

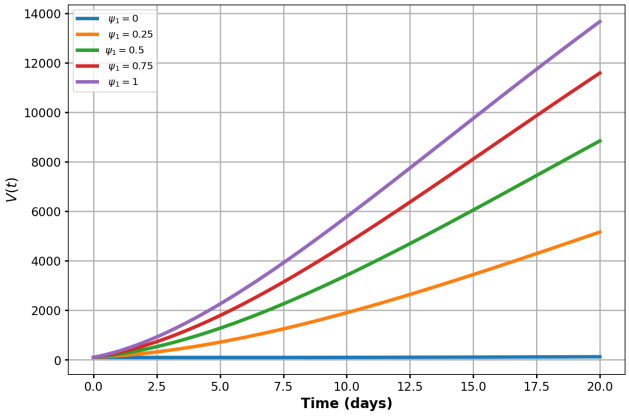

(c) Bacterial concentration (B)

Figure 4. Impact of children vaccination on model variables. Subfigures (a)–(c) show the influence of vaccination rate (ψ_1) among children on susceptible population, infection levels, and bacterial concentration, respectively

Integrating and applying the initial conditions gives the first-order solutions:

$$\begin{aligned}
S_{C1}(t) &= \big[\Lambda_C - (1-\omega)\lambda_C B_0(S_{C0}+S_{A0}) - (\mu+\psi_1+g)S_{C0} \\
&\quad + \rho_1 V_0\big]t, \\
S_{A1}(t) &= \big[\Lambda_A - (1-\omega)\lambda_A B_0(S_{C0}+S_{A0}) - (\mu+\psi_2)S_{A0} \\
&\quad + gS_{C0} + \rho_2 V_0\big]t, \\
V_1(t) &= \big[\psi_1 S_{C0} + \psi_2 S_{A0} - (\rho_1+\rho_2+\mu)V_0\big]t, \\
I_1(t) &= \big[(1-\omega)B_0(S_{C0}+S_{A0})(\lambda_C+\lambda_A) - (\mu+\delta+\tau)I_0\big]t, \\
T_1(t) &= \big[\tau I_0 - (\varepsilon+\mu)T_0\big]t, \\
R_1(t) &= \big[\varepsilon T_0 - \mu R_0\big]t, \\
B_1(t) &= \big[(1-\omega)\eta I_0 - \upsilon B_0\big]t.
\end{aligned}$$

3.7.3. Second-Order Approximation

Proceeding similarly for $n = 2$, the second-order derivatives yield expressions of the form

$$\frac{dS_{C2}}{dt} = f_C(t), \quad \frac{dS_{A2}}{dt} = f_A(t),$$

$$\frac{dV_2}{dt} = f_V(t), \quad \frac{dI_2}{dt} = f_I(t),$$

where each $f_i(t)$ is derived by substituting the first-order terms into the nonlinear parts of the model. Integrating, the second-order solutions take the form:

$$S_{C2}(t) = \tfrac{1}{2}f_C(t)t^2, \quad S_{A2}(t) = \tfrac{1}{2}f_A(t)t^2, \quad V_2(t) = \tfrac{1}{2}f_V(t)t^2,$$

$$I_2(t) = \tfrac{1}{2}f_I(t)t^2, \quad T_2(t) = \tfrac{1}{2}f_T(t)t^2, \quad R_2(t) = \tfrac{1}{2}f_R(t)t^2,$$

$$B_2(t) = \tfrac{1}{2}f_B(t)t^2.$$

3.7.4. Approximate Series Solution

Summing the first three terms of the HPM series yields the second-order approximate solution:

$$\begin{aligned}
S_C(t) &\approx S_{C0}(t) + S_{C1}(t) + S_{C2}(t), \\
S_A(t) &\approx S_{A0}(t) + S_{A1}(t) + S_{A2}(t), \\
V(t) &\approx V_0(t) + V_1(t) + V_2(t), \\
I(t) &\approx I_0(t) + I_1(t) + I_2(t), \\
T(t) &\approx T_0(t) + T_1(t) + T_2(t), \\
R(t) &\approx R_0(t) + R_1(t) + R_2(t), \\
B(t) &\approx B_0(t) + B_1(t) + B_2(t).
\end{aligned}$$

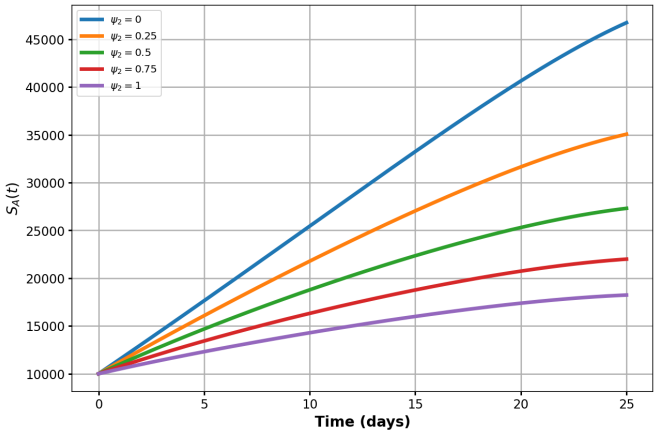

(a) Susceptible adults (S_A)

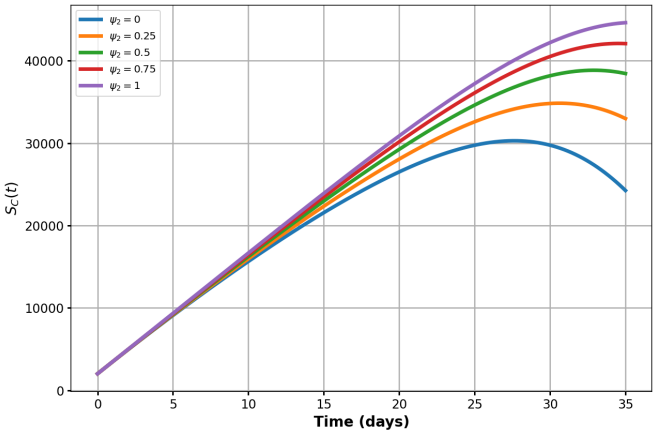

(b) Infected individuals (I)

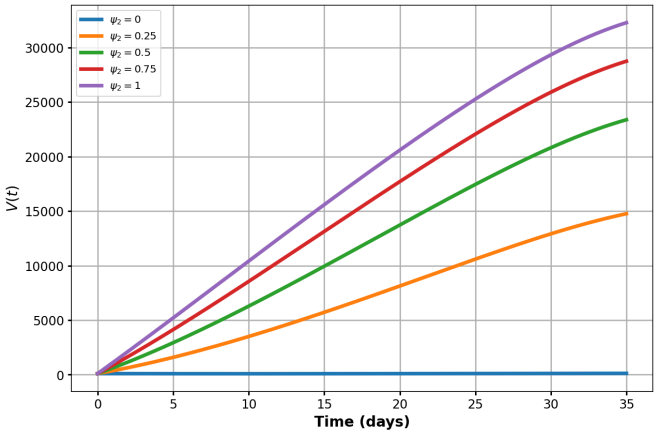

(c) Bacterial concentration (B)

Figure 5. Impact of adult vaccination on model variables. Subfigures (a)–(c) show the influence of vaccination rate (ψ_2) among adults on susceptible population, infection prevalence, and bacterial concentration respectively

These approximate solutions can then be evaluated numerically using parameter values provided in Table 2 to analyze the impact of vaccination, hygiene, and treatment parameters on typhoid dynamics.

3.8. Numerical Simulation

To assess the validity and accuracy of the Homotopy Perturbation Method (HPM) applied to the proposed typhoid fever model, the approximate analytical solutions obtained via HPM were benchmarked against numerical solutions generated using the standard fourth-order Runge–Kutta (RK4) method. Since HPM provides a local approximation, the comparison was conducted over a short time interval where its convergence is expected to be reliable. Figure 3 presents the relative error between the HPM and RK4 solutions for the infected population and bacterial concentration. Throughout the validation interval, the error remains small and bounded, indicating strong agreement between the two approaches and confirming the reliability and correctness of the HPM approximation for the proposed model.

Figure 3 presents the relative error between the Homotopy Perturbation Method (HPM) approximate solutions and the numerical Runge–Kutta solutions for the infected population and bacterial concentration. The error remains small and bounded over the considered time interval, indicating strong agreement between the two methods. This confirms the reliability and accuracy of the HPM approximation for capturing the short-term dynamics of the model.

Figure 4 illustrates the effect of increasing the vaccination rate among children (ψ_1) on the model dynamics. As ψ_1 increases, the susceptible adult population decreases, indicating reduced transmission from children to adults. In addition, higher child vaccination rates lead to a noticeable reduction in infection prevalence and environmental bacterial concentration. This demonstrates the indirect protective effect of vaccinating children through herd immunity, which lowers overall disease transmission in the population.

Figure 5 shows the impact of increasing the adult vaccination rate (ψ_2) on disease dynamics. Increasing ψ_2 results in a faster decline in infection prevalence and a reduction in bacterial concentration in the environment. The susceptible adult population also decreases as vaccination coverage improves. These results highlight the direct effectiveness of adult vaccination and emphasize the importance of age-specific vaccination strategies for effective typhoid fever control.

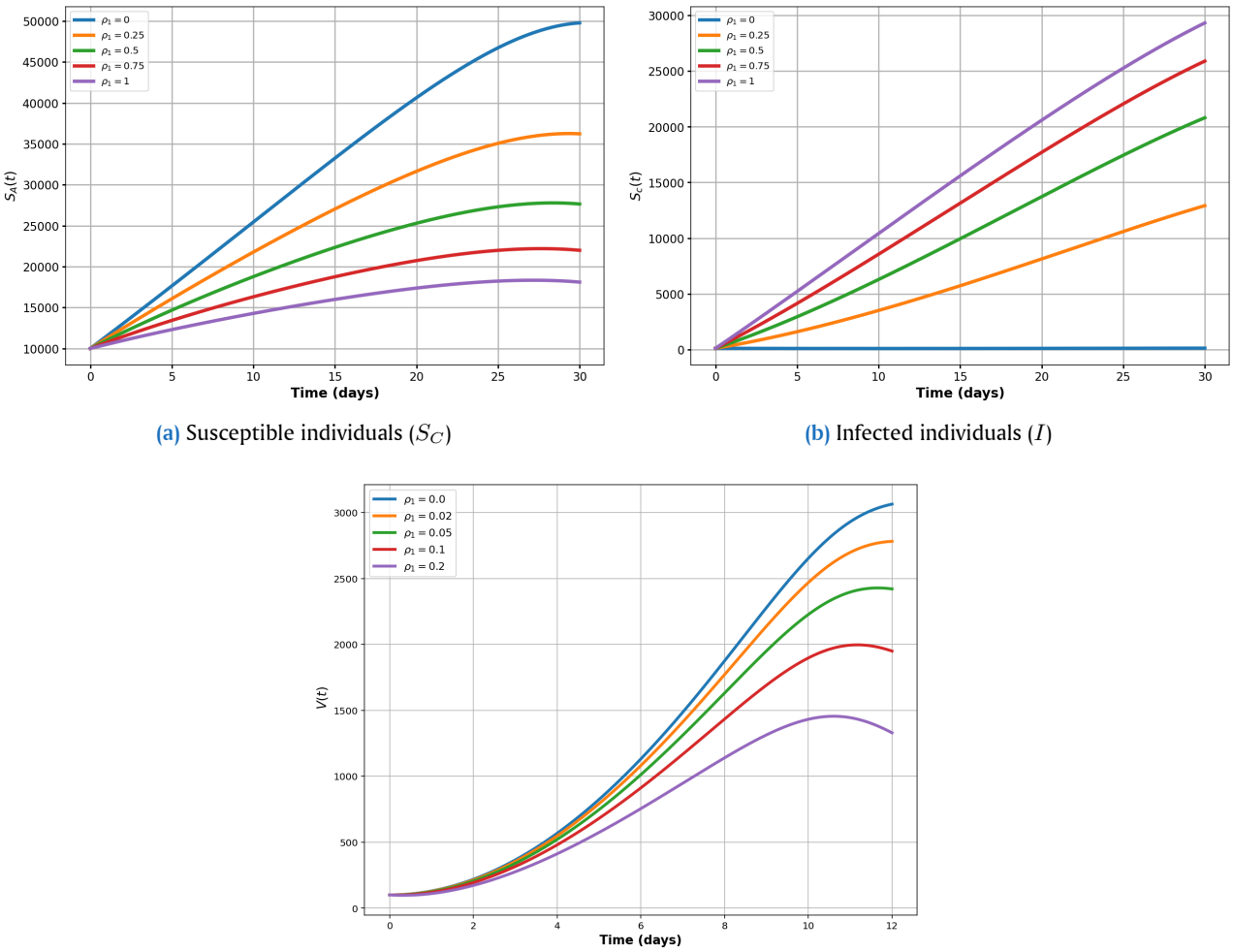

(a) Susceptible individuals (S_C)

(b) Infected individuals (I)

(c) Bacterial concentration (B)

Figure 6. Impact of the waning rate of children vaccination (ρ_1) on model variables. An increase in ρ_1 reduces long-term immunity among children, leading to higher infection prevalence and sustained bacterial concentration

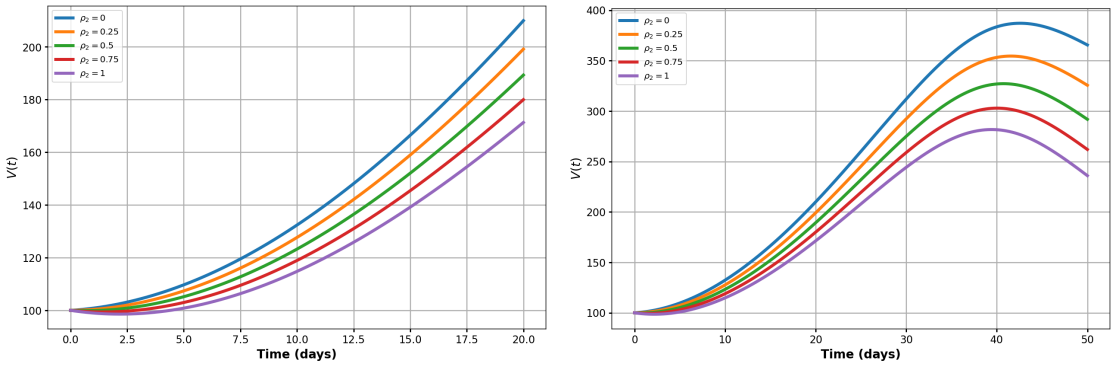

(a) Susceptible adults (S_A)

(b) Infected individuals (I)

Figure 7. Impact of the waning rate of adult vaccination (ρ_2) on model variables. Higher values of ρ_2 increase the risk of reinfection and prolong bacterial persistence

Figure 6 illustrates the effect of increasing the waning rate of immunity among children (ρ_1) on the model dynamics. As ρ_1 increases, immunity acquired through vaccination diminishes more rapidly, leading to an increase in the susceptible children population. This loss of protection results in higher infection levels and a sustained concentration of bacteria in the environment. The figure demonstrates that rapid waning of immunity among children can undermine long-term disease control and contribute to recurrent outbreaks.

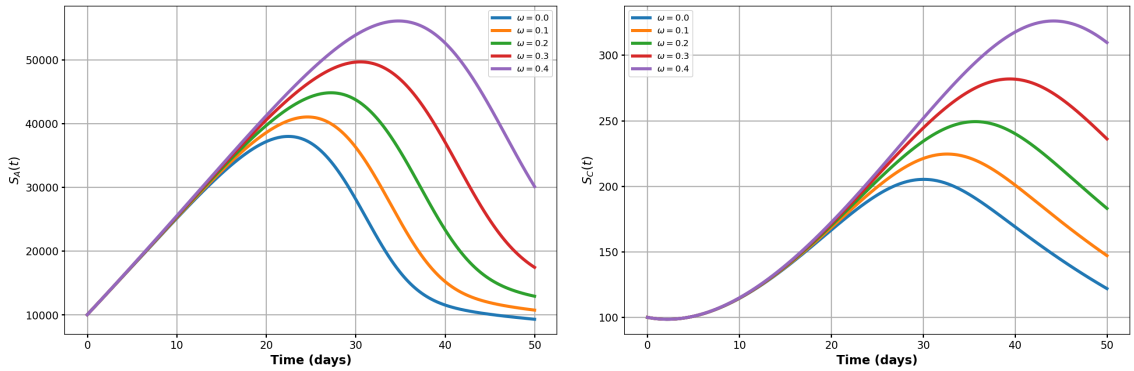

(a) Susceptible individuals (S_C) **(b)** Bacterial concentration (B)

Figure 8. Impact of hygienic practices on model variables. Improved hygiene reduces infection and lowers bacterial levels in the environment

Figure 7 shows the impact of increasing the waning rate of immunity among adults (ρ_2) on disease dynamics. Higher values of ρ_2 increase the number of susceptible adults over time, thereby elevating the risk of reinfection and prolonging bacterial persistence in the environment. This reduction in long-term vaccine effectiveness highlights the need for booster vaccination programs among adults to maintain immunity and sustain low infection prevalence levels in the population.

Figure 8 shows that improving hygiene reduces infection prevalence and bacterial concentration but has a limited impact on overall susceptibility levels. While hygiene practices alone do not provide complete protection, they complement vaccination by curbing environmental transmission. The model therefore emphasizes that a combined strategy—integrating improved hygiene, vaccination, and booster programs—is critical for effective typhoid fever control. This integrated approach offers a practical framework for reducing disease burden and guiding public health policies in endemic regions.

4. Conclusion

This study demonstrates that incorporating age structure into the mathematical modeling of typhoid fever provides deeper insights into disease transmission and control. The results reveal that targeted vaccination and treatment strategies for specific age groups significantly reduce infection rates and improve health outcomes. Sensitivity analysis identifies vaccination coverage, treatment efficacy, and waning immunity rates as key parameters driving disease dynamics. Overall, the model offers a robust analytical framework to support public health decision-making, particularly in resource-limited settings, and underscores the effectiveness of age-specific intervention strategies in managing typhoid fever. The findings of this research highlight the importance of implementing age-specific vaccination and treatment strategies for controlling typhoid fever. Public health programs should prioritize booster doses to counteract waning immunity and promote widespread hygiene education to minimize environmental transmission. Future studies should extend the current model to incorporate environmental, behavioral, and socioeconomic factors that influence disease dynamics. Such extensions will enhance the model's predictive accuracy and provide valuable insights for designing sustainable and context-sensitive disease control strategies.

Author Contributions. **Mutairu Kayode Kolawole**: Conceptualization, methodology, formal analysis, supervision. **Rasheed Gbemisola Ayoola**: Software, validation, data curation, visualization. **Folasade Ajimot Adebisi**: Investigation, resources, writing—review and editing. All authors discussed the results and actively participated in drafting, revising, and approving the final manuscript.

Acknowledgement. The author would like to thank the editors and reviewers for their insightful comments and helpful suggestions that significantly improved the quality of this manuscript.

Funding. The author received no funding for this study.

Conflict of interest. The authors declare no conflict of interest.

Data availability. Not applicable.

References

[1] V. Keshav, N. Potgieter, and T. Barnard, "Detection of vibrio cholerae o1 in animal stools collected in rural areas of the limpopo province," *Water SA*, vol. 36, no. 2, p. 167, 2019, doi: 10.4314/wsa.v36i2.183724.

[2] O. J. Peter, A. F. Adebisi, M. O. Ajisope, F. O. Ajibade, A. I. Abioye, and F. A. Oguntolu, "Global stability analysis of typhoid fever model," *Advances in Systems Science and Applications*, vol. 20, no. 2, 2020, doi: 10.25728/assa.2020.20.2.792.

[3] T. A. Ayoola, H. O. Edogbanya, O. J. Peter, F. A. Oguntolu, K. Oshinubi, and M. L. Olaosebikan, "Modelling and optimal control analysis of typhoid fever," *Journal of Mathematics and Computer Science (J. Math. Comput. Sci.)*, vol. 11, no. 6, pp. 6666–6682, 2021.

[4] P. O. James and M. O. Ibrahim, "Application of variational iteration method in solving typhoid fever model," in *2019 Big Data, Knowledge and Control Systems Engineering (BdKCSE)*, Sofia, Bulgaria, 2019, pp. 1–5, doi: 10.1109/BdKCSE48644.2019.9010598.

[5] O. J. Peter, M. O. Ibrahim, H. O. Edogbanya, F. A. Oguntolu, K. Oshinubi, A. A. Ibrahim, T. A. Ayoola, and J. O. Lawal, "Direct and indirect transmission of typhoid fever model with optimal control," *Results in Physics*, vol. 27, p. 104463, 2021, doi: 10.1016/j.rinp.2021.104463.

[6] A. S. Shaikh and K. S. Nisar, "Transmission dynamics of fractional order typhoid fever model using caputo–fabrizio operator," *Chaos, Solitons & Fractals*, vol. 128, pp. 355–365, 2019, doi: 10.1016/j.chaos.2019.08.012.

[7] F. Dayan, N. Ahmed, A. H. Ali *et al.*, "Numerical investigation of a typhoid disease model in fuzzy environment," *Scientific Reports*, vol. 13, p. 21993, 2023, doi: 10.1038/s41598-023-48405-w.

[8] J. I. Irunde, J. Z. Ndendya, J. A. Mwasunda, and P. K. Robert, "Modeling the impact of screening and treatment on typhoid fever dynamics in un-

protected population," *Results in Physics*, vol. 54, p. 107120, 2023, doi: 10.1016/j.rinp.2023.107120.

[9] S. Edward and N. Nyerere, "Modelling typhoid fever with education, vaccination and treatment," *International Journal of Theoretical and Applied Mathematics*, vol. 2, no. 2, 2017, doi: 10.11648/j.ijtam.20160202.30.

[10] P. Bwalya, E. S. Solo, J. Y. Chizimu, D. Shrestha, G. Mbulo, J. Thapa, C. Nakajima, and Y. Suzuki, "Characterization of embb mutations involved in ethambutol resistance in multi-drug resistant mycobacterium tuberculosis isolates in zambia," *Tuberculosis*, vol. 133, p. 102184, 2022, doi: 10.1016/j.tube.2022.102184.

[11] G. Dougan and S. Baker, "Salmonella enterica serovar typhi and the pathogenesis of typhoid fever," *Annual Review of Microbiology*, vol. 68, no. 1, pp. 317–336, 2014, doi: 10.1146/annurev-micro-091313-103739.

[12] M. Amouch and N. Karim, "Mathematical modeling of covid-19 and omicron outbreak spread: Optimal control approach for intervention strategies," *Optimal Control Applications and Methods*, vol. 44, no. 5, pp. 2916–2937, 2023, doi: 10.1002/oca.3019.

[13] M. K. Kolawole, K. A. Odeyemi, A. O. Oladapo, and K. A. Bashiru, "Dynamical analysis and control strategies for capturing the spread of covid-19," *Tanzania Journal of Science*, vol. 48, no. 3, pp. 680–690, 2022, doi: 10.4314/tjs.v48i3.15.

[14] R. Kuehn, N. Stoesser, D. Eyre, T. C. Darton, B. Basnyat, and C. M. Parry, "Treatment of enteric fever (typhoid and paratyphoid fever) with cephalosporins," *Cochrane Database of Systematic Reviews*, no. 11, 2022, doi: 10.1002/14651858.cd010452.pub2.

[15] A. El-Mesady, A. Elsonbaty, and W. Adel, "Stability analysis and optimal control strategies of a fractional-order monkeypox virus infection model," *Physica Scripta*, vol. 98, no. 9, p. 095256, 2023, doi: 10.1088/1402-4896/acf16f.

[16] ——, "On nonlinear dynamics of a fractional order monkeypox virus model," *Chaos, Solitons & Fractals*, vol. 164, p. 112716, 2022, doi: 10.1016/j.chaos.2022.112716.

[17] A. Ahmad, U. Atta, M. Farman, K. S. Nisar, H. Ahmad, and E. Hincal, "Investigation of lassa fever with relapse and saturated incidence rate: Mathematical modeling and control," *Modeling Earth Systems and Environment*, vol. 11, no. 3, p. 202, 2025, doi: 10.1007/s40808-025-02370-7.

[18] M. Farman, A. Ahmad, U. Atta, K. S. Nisar, and A. Ghaffar, "Hyers–ulam stability and bifurcation control of leptospirosis disease dynamics and preventions: Modeling with singular and non-singular kernels," *PLoS ONE*, vol. 20, no. 3, p. e0314095, 2025, doi: 10.1371/journal.pone.0314095.

[19] F. K. Alalhareth, U. Atta, A. H. Ali, and M. H. Alharbi, "Analysis of leptospirosis transmission dynamics with environmental effects and bifurcation using fractional-order derivative," *Alexandria Engineering Journal*, vol. 80, pp. 372–382, 2023, doi: 10.1016/j.aej.2023.08.063.

[20] B. Liu, "Analysis on the current situation, problems and potential solutions for the chinese precious metals futures market," *BCP Business & Management*, vol. 38, pp. 1239–1244, 2023, doi: 10.54691/bcpbm.v38i.3852.

[21] A. Manesh, E. Meltzer, C. Jin, C. Britto, D. Deodhar, S. Radha, E. Schwartz, and P. Rupali, "Typhoid and paratyphoid fever: a clinical seminar," *Journal of Travel Medicine*, vol. 28, no. 3, 2021.

[22] V. G. Melnikov, A. Berger, A. Dangel, and A. Sing, "Lateral flow immunoassay-based laboratory algorithm for rapid diagnosis of diphtheria," *Open Research Europe*, vol. 3, p. 62, 2023, doi: 10.12688/openreseurope.15038.1.

[23] B. Muchmore, P. Muchmore, C. W. Lee, M. E. Alarcón-Riquelme, and A. Muchmore, "Tracking potential covid-19 outbreaks with influenzalike symptoms urgent care visits," *Pediatrics*, vol. 146, no. 4, 2020, doi: 10.1542/peds.2020-1798.

[24] D. Muthuirulandi Sethuvel, N. Devanga Ragupathi, S. Anandan, B. Veeraraghavan, and L. Sangal, "Molecular epidemiology of c. diphtheriae shows rapid evolution of strains in india: An update from national diphtheria surveillance network," *International Journal of Infectious Diseases*, vol. 101, p. 372, 2020, doi: 10.1016/j.ijid.2020.09.978.

[25] N. Lawal, S. A. Abdullahi, and D. S. Abolude, "Physicochemical characteristics and fish abundance and diversity of mairua reservoir water, funtua, katsina state, north-western nigeria," *Journal of Applied Sciences and Environmental Management*, vol. 27, no. 1, pp. 125–132, 2023, doi: 10.4314/jasem.v27i1.18.

[26] M. Kolawole, A. Oluwarotimi, K. Odeyemi, and A. Popoola, "Analysis of corona-virus mathematical model in asymptomatic and symptomatic cases with vaccine using homotopy perturbation method," *Journal of Applied Computer Science & Mathematics*, vol. 17, no. 1, pp. 20–27, 2023, doi: 10.4316/jacsm.202301003.

[27] E. I. Komarovskaya and V. Perelygyna, "Assay of diphtheria vaccine potency by intradermal challenge test," *Epidemiology and Vaccinal Prevention*, vol. 22, no. 4, pp. 12–23, 2023, doi: 10.31631/2073-3046-2023-22-4-12-23.

[28] J. M. Heffernan, R. J. Smith, and L. M. Wahl, "Perspectives on the basic reproductive ratio," *Journal of the Royal Society Interface*, vol. 2, no. 4, pp. 281–293, 2005, doi: 10.1098/rsif.2005.0058.

[29] O. Diekmann, J. A. P. Heesterbeek, and M. G. Roberts, "The construction of next-generation matrices for compartmental epidemic models," *Journal of the Royal Society Interface*, vol. 7, no. 47, pp. 873–885, 2010, doi: 10.1098/rsif.2009.0386.

[30] P. van den Driessche and J. Watmough, "Reproduction numbers and subthreshold endemic equilibria for compartmental models of disease transmission," *Mathematical Biosciences*, vol. 180, no. 1–2, pp. 29–48, 2002, doi: 10.1016/S0025-5564(02)00108-6.

[31] O. J. Peter, H. S. Panigoro, A. Abidemi, M. M. Ojo, and F. A. Oguntolu, "Mathematical model of covid-19 pandemic with double dose vaccination," *Acta Biotheoretica*, vol. 71, no. 2, p. 9, 2023, doi: 10.1007/s10441-023-09460-y.

[32] M. Z. Ndii and Y. A. Adi, "Modelling the transmission dynamics of covid-19 under limited resources," *Commun. Math. Biol. Neurosci.*, vol. 2020, pp. Article–ID, 2020.

[33] M. D. Miller-Dickson, V. A. Meszaros, S. Almagro-Moreno, and C. B. Ogbunugafor, "Hepatitis c virus modelled as an indirectly transmitted infection highlights the centrality of injection drug equipment in disease dynamics," *Journal of the Royal Society Interface*, vol. 16, no. 158, p. 20190334, 2019, doi: 10.1098/rsif.2019.0334.